



# CHORUS

This is the accepted manuscript made available via CHORUS. The article has been published as:

## Redshift in the Optical Absorption of ZnO Single Crystals in the Presence of an Intense Midinfrared Laser Field

Shambhu Ghimire, Anthony D. DiChiara, Emily Sistrunk, Urszula B. Szafruga, Pierre Agostini, Louis F. DiMauro, and David A. Reis

Phys. Rev. Lett. **107**, 167407 — Published 14 October 2011

DOI: [10.1103/PhysRevLett.107.167407](https://doi.org/10.1103/PhysRevLett.107.167407)

# Strong-field electroabsorption near the limit of crystal bonding

Shambhu Ghimire,<sup>1,\*</sup> Anthony D. DiChiara,<sup>2</sup> Emily Sistrunk,<sup>2</sup> Urszula B. Szafruga,<sup>2</sup> Pierre Agostini,<sup>2</sup> Louis F. DiMauro,<sup>2</sup> and David A. Reis<sup>1,3,†</sup>

<sup>1</sup>*PULSE Institute, SLAC National Accelerator Laboratory, Menlo Park, CA, 94025, USA*

<sup>2</sup>*Physics Department, Ohio State University, Columbus, OH, 43210, USA*

<sup>3</sup>*Departments of Photon Science and Applied Physics, Stanford University, Stanford, CA, 94305, USA*

We report time-resolved electroabsorption of a weak probe in a 500  $\mu\text{m}$  thick zinc-oxide crystal in the presence of strong mid-infrared pump in the tunneling limit. We observe a substantial redshift in the absorption edge that scales with the cube root of intensity up to 1  $\text{TW}/\text{cm}^2$  ( $0.38 \text{ eV cm}^{2/3}\text{TW}^{-1/3}$ ) after which it increases more slowly to 0.4 eV at a maximum applied intensity of 5  $\text{TW}/\text{cm}^2$ . The maximum shift corresponds to more than 10% of the band-gap. The change in scaling occurs in a regime of nonperturbative high-order harmonic generation where electrons undergo periodic Bragg scattering from the Brillouin zone boundaries. It also coincides with the limit where the electric field becomes comparable to the ratio of the band-gap to the lattice spacing.

PACS numbers: 72.20.Ht, 42.65.Ky, 78.47.-p

The response of solids to strong electromagnetic radiation in the limit when the electric field amplitude approaches the ratio of the band-gap to the lattice spacing remains relatively unexplored. In Ghimire et al. [1] the response of a single crystal ZnO to a strong field mid-infrared (MIR) laser was demonstrated to produce high-order harmonics that could not be treated within a perturbative framework. Here, the field cannot be thought of as producing a small perturbation to the Hamiltonian, and thus the basic characteristics of the solid in the presence of the field may be altered dramatically. While the high harmonic generation (HHG) is consistent with a simple and intuitive two-step model comprising tunneling between valence and conduction states and radiation from the acceleration of carriers within a band. The results raise important questions about the electronic structure of the crystal in the strong field limit.

Non-resonant below threshold ionization was considered theoretically by Keldysh [2] in 1964. In the case of insulating crystals, he presented a unified model for the coupling between valence and conduction band states in terms of the dimensionless adiabatic parameter  $\gamma$  which is the ratio of the characteristic tunneling time to the laser period. The model considered parabolic bands such that  $\gamma = (\epsilon_g/4U_p^*)^{1/2}$  where,  $\epsilon_g$  is the band-gap and  $U_p^*$  is the ponderomotive energy of the electrons and holes of reduced effective mass  $m^*$ . In the multiphoton limit,  $\gamma \gtrsim 1$ , the coupling can be treated perturbatively in the intensity. In the perturbative limit various nonlinear phenomena such as harmonic generation and multiple wave mixing effects in the form of sideband generation and below gap electroabsorption have been observed [4–7]. In particular, the electroabsorption of near band-gap radiation in the presence of a strong driving laser field (high frequency, or dynamical Franz-Keldysh effect) has been investigated both theoretically [8–12] and experimentally [5, 7] up to the case when  $U_p^* \sim \hbar\omega$ , the drive photon energy. However, when  $U_p^*$  exceeds both  $\hbar\omega$  and  $\epsilon_g$ , we enter into a new regime where the interactions depend on the instantaneous field strength [13, 14], i.e. the tunneling regime ( $\gamma \ll 1$ ) [15].

In this Letter we present measurements of the electroabsorption of ZnO driven by a strong mid-infrared laser pulse in the nonperturbative limit when the ponderomotive energy is greater than both the photon energy and band-gap, and the crystal bonding limit where the width of the tunneling barrier is on order of the lattice spacing. We observe a substantial intensity dependent redshift of the absorption edge using a weak broad band optical probe. The redshift scales with the cube-root of MIR intensity up to  $1 \text{ TW/cm}^2$ , consistent with photon assisted tunneling in the instantaneous laser field. The redshift begins to saturate above this intensity—at the same level that we observe a change in the scaling of the harmonics emission[1]. We attribute these results to nonparabolic band effects which appear to play a defining role in the strong-field induced intra- and interband electron dynamics.

In the experiments, we excite a  $500 \mu\text{m}$  thick c-cut single crystal ZnO with a linearly polarized MIR laser and measure its near band-edge optical absorption using a broadband pulse in a pump-probe geometry as shown in Fig. 1(a). The crystal and laser system are the same as used in Ghimire et al. [1]. The MIR laser pulses are produced by difference frequency generation (DFG) between a femtosecond Ti:sapphire laser and a picosecond Nd:YLF laser, providing over  $100 \mu\text{J}$  per  $100 \text{ fs}$  ( $\sim 9$  cycle) pulse centered at  $3.25 \mu\text{m}$  at  $1 \text{ kHz}$ [16]. The MIR beam is focused near the exit face of the sample at near normal incidence using  $f/3$  optics so that the Rayleigh range is about  $100 \mu\text{m}$ , substantially less than the crystal thickness. The maximum incident intensity without imposing physical damage is  $\sim 5 \text{ TW/cm}^2$  [1]. The advantage of using long wavelength laser compared to near infrared is two-fold: first, the smaller photon energy, approximately one tenth of the gap ( $\sim 3.35 \text{ eV}$  [17, 18]), corresponds to a much lower photoabsorption cross section for the same intensity leading to a higher damage threshold; and second, the ponderomotive energy scales quadratically with wavelength [19].

To produce the broadband optical probe a portion of the Ti:sapphire beam is picked off before DFG and frequency doubled in a thin BBO crystal. After removing the residual fundamental with a short pass filter (Schott BG39), the beam is focused into a sapphire plate broadening the spectrum to  $>0.6 \text{ eV}$  ( $1/e^2$ ) centered around  $3 \text{ eV}$ . The broadband near band-gap light is apertured and subsequently focused on the sample at  $\sim 18$  degrees to normal incidence with its polarization in the same plane as that of the MIR. The spot size of both pump and probe beams are comparable at the sample. The pulse energy of the probe is about  $15 \text{ nJ}$ , low enough that we do not observe nonlinear effects of the probe. A translation stage is used to change the time delay of the probe. The transmitted probe beam is collected by  $f/4$  optics onto the slit of an imaging spectrometer with an intensified CCD detector, and the reflected probe beam is monitored with a photodiode. In order to minimize the effects of spatial nonuniformity of the pump, the central portion of the transmitted probe is selected by a combination of an aperture just after the sample and a finite integration range in the non-dispersed direction on the CCD. Figure 1(b) shows dramatic modification of the transmission of the broadband light as it overlaps in time with the strong MIR pulse inside the crystal at an estimated intensity of  $1 \text{ TW/cm}^2$ . There was no measurable change in the reflection of the probe, such that the decrease in transmission is due to increased absorption. Negative time delays correspond to the probe arriving before the pump at the exit surface. The field induces almost complete absorption of the probe light only when the pulses are overlapped temporally inside the crystal. The transient nature of the process means that band-filling effects due to direct tunneling can be neglected. The overlap of the two pulses in the crystal occurs over a few picoseconds due to the difference in group velocity of the MIR and probe light and the finite pulse durations. This corresponds to on

order of 2–3 Rayleigh range of MIR. However, the maximum extent of the electroabsorption is expected to occur at the peak of MIR pulse and over an effective interaction length on order of the Rayleigh range. Strong group velocity dispersion near the band-gap causes the different spectral content of the broadband probe to overlap with the MIR pulse at the exit face at slightly different time delays, as the frequency components closest to the band edge travel much slower than the MIR.

We study the intensity dependence of the MIR field induced optical absorption. For the intensity range studied,  $0.15 < \gamma < 2$ , and  $35 \text{ eV} > U_p^* > 0.2 \text{ eV}$  assuming an effective mass  $m^* = 0.13m_e$ [20]. We set the pump-probe delay for maximum absorption, corresponding to overlap between the pump and probe ( $t = 0$  in Fig. 1(b) near the exit face of the crystal where the MIR laser is focused. This means that the bluer portion of the probe (nearer the band-gap) sees a smaller field than the redder, and consequently at lower intensities the red shift could be slightly underestimated. Figure 2(a) shows the absorption coefficient,  $\alpha$ , measured with a UV-visible spectrophotometer. The figure clearly shows the onset of the field free absorption edge near 3.2 eV. Above this photon energy the measurement is limited by the strong absorption in the thick crystal and finite dynamic range of the detector. In Fig. 2(b) we plot the relative change in the integrated absorbance (base-10), for four peak intensities from  $I = 0.1 \text{ TW/cm}^2$  to  $5 \text{ TW/cm}^2$ . The origin of the strong dip at  $\sim 3.05 \text{ eV}$  is due to fluorescence and is also seen in the HHG spectra. At the highest intensity we observe  $\sim 90\%$  reduction in the transmission of the probe beam. We also see no crystal orientation dependence on the absorption for rotation about the c-axis. The field induced absorption edge is indicated with a vertical arrow in Fig. 2(b) as determined by the point at which the field modified absorption spectra deviate significantly from the field-free case. We plot the redshift in the absorption edge ( $\hbar\Delta\Omega_E$ ) as function of the MIR intensity in Fig. 3(a). The data can be fit to a single power law for  $I \leq 1 \text{ TW/cm}^2$  as  $\hbar\Delta\Omega_E = 0.38\text{eV}(I[\text{TW/cm}^2])^{1/3}$  (dashed line). As discussed below, the cube-root scaling is what is expected for the induced redshift in the DC limit (Franz-Keldysh effect)[21, 22] consistent with (photon-assisted) tunnel ionization in the instantaneous field of the MIR laser. For intensities,  $I > 1 \text{ TW/cm}^2$ , we observe a saturation in  $\hbar\Delta\Omega_E$ . While the redshift saturates, both the spectrally integrated absorption of the probe and the direct tunneling of the MIR continue to grow. The latter is evidenced by observation of a continuous increase in both the fluorescence and HHG yields with increasing MIR intensity (in the absence of the probe light). The HHG yield is shown in Fig. 3(b) on a logarithmic scale. The inset is a representative harmonic spectrum at the MIR intensity of  $5 \text{ TW/cm}^2$ . The yield for various harmonic orders (labeled HO in the figure) shows two regimes with different intensity scaling: for  $I < 1 \text{ TW/cm}^2$ , the yield increases at approximately as the tenth order of the intensity while for  $I > 1 \text{ TW/cm}^2$  it scales as less than the second order in intensity. Notably the redshift deviates from cube-root scaling at the same intensity where the HHG also changes scaling, represented by the shaded regions in Fig. 3.

The observed cube-root intensity scaling below  $1 \text{ TW/cm}^2$  is indicative of a tunneling-like process, where the transition rate depends on the instantaneous electric field. In the tunneling limit, we do not expect any drive frequency dependence of the transition rate for either direct or photon assisted processes (electroabsorption) in order that they connect smoothly to the DC case. In this case, and under the simplifying assumptions of a constant effective mass and a sharp absorption edge, the photon-assisted transition rate as a function of electric field  $E$  and optical

photon energy  $\hbar\Omega$  is

$$w(E, \Omega) = C \exp \left\{ -\frac{4\sqrt{2m^*}}{3e\hbar E} (\epsilon_g - \hbar\Omega)^{3/2} \right\}, \quad \hbar\Omega < \epsilon_g, \quad (1)$$

where the prefactor,  $C$ , is a relatively slowly varying function of  $E$  and  $\Omega$  compared to the exponential over the region of validity  $\sqrt{m^*}(\epsilon_g - \hbar\Omega)^{3/2} \gtrsim e\hbar E$  [21]. Thus, the redshift,  $\Delta\Omega_E \propto E^{2/3}$  (i.e.  $I^{1/3}$ ). We note that in the dynamical case [8, 23] the transitions are due to two photon absorption ( $\omega + \Omega$ ) and the below gap absorption scales bi-linearly in the pump and probe. We do not observe any evidence of frequency mixing processes such as sidebands ( $\Omega \pm n\omega$ ) on the optical probe, providing further proof of a tunneling (as opposed to a multiphoton) process.

At intensities above 1 TW/cm<sup>2</sup>, our data no longer follow a cube-root intensity scaling, although we expect to be even deeper into the tunneling regime. Here the electrons and holes traverse the entire Brillouin zone within a single half-cycle of the laser pulse. This is the same regime where, the nonperturbative high order harmonics are believed to be due to radiation from multiple Bragg scattering of carriers that have tunnel ionized in the MIR field. [1]. The rates for both direct and photon assisted tunneling depends on the energy difference between the valence and conduction band states of the same momentum and their (field-free) transition dipole matrix elements. Thus, at intensities where Bloch oscillations occur, we expect non-parabolic effects to play an important role in the tunneling process [10]. Furthermore, if we naively calculate the ponderomotive energy in the effective mass approximation at the intensity where the redshift begins to saturate, we find  $U_p^* \sim 7$  eV well exceeding  $\hbar\omega$  (0.38 eV),  $\epsilon_g$  (3.35 eV) and even the conduction band width ( $\Delta_c \sim 5$  eV [20]). Thus, in the context of the failure of the effective mass model, it is not surprising that the redshift would deviate from the one-third scaling above this level.

Non-parabolic effects also enter into the ponderomotive energy. Taking into account dispersion in the effective mass, the ponderomotive energy for a cosine band,  $U_p(k) = \Delta \cos(kd)[1 - J_0(\omega_B/\omega)]/2$ , where  $\Delta$  is the sum of the valence and conduction bandwidths,  $d$  is the lattice spacing,  $\hbar k$  is the crystal momentum, and  $\omega_B = eEd/\hbar$  is the angular frequency at which carriers traverse the Brillouin zone (Bloch frequency) for a peak DC field  $E$  in the absence of scattering. For small fields where  $\omega_B \ll \omega$  this reduces to  $U_p^* = e^2 E^2 / 4m^* \omega^2$ , i.e., the atomic case for an (reduced electron-hole) effective mass,  $m^*$  [19]. However, as the field increases,  $U_p$  becomes constrained by the bandwidth and shows oscillatory behavior. In this limit, Gruzdev [10] calculates the direct tunneling rate for cosine bands and finds a suppression relative to Keldysh [2]. The calculated rate approaches zero just below  $\omega_B/\omega = 2.4048\dots$ , i.e., the first zero of  $J_0(\omega_B/\omega)$  and diverges just above. This intensity corresponds to the case where the sum of the band energy and ponderomotive energy becomes flat throughout the Brillouin zone. It is also comparable to the intensity where we see the transition in both electroabsorption and the HHG yield ( $\omega_B/\omega \sim 2$ , for  $d = 2.8\text{\AA}$ ). Gruzdev goes on to predict that this (first) divergence of the rate corresponds to the threshold for material breakdown. In our experiments we are able to exceed this limit by nearly a factor of two ( $\omega_B/\omega \sim 4.5$ ) before damage. At some point a simple two band picture of the solid will break down. We note that the effect of nonparabolic and multiple bands has been considered theoretically in the case of the (weak field) DC Franz-Keldysh effect [24], but to the best of our knowledge it has not been considered in the limit where the field competes with bonding.

In conclusion, we have observed strong electroabsorption in a ZnO single crystal pumped by an ultrafast MIR laser in the strong-field nonperturbative limit where the ponderomotive energy exceeds the drive photon energy and

the electron bandwidth, and the electric field approaches the ratio of the band-gap to the lattice constant. We measure a redshift in the absorption edge of more than a tenth of the band-gap that exists only during the overlap of the MIR drive laser and the optical probe inside the sample. The effect scales as the cube-root of intensity, as expected for photon-assisted tunneling in the effective mass approximation, up to a regime where nonparabolic effects become important, and Bragg scattering occurs within a half cycle of the MIR laser. This is the same regime where nonperturbative high-order harmonics are produced and are attributed to nonlinear acceleration of tunnel ionized electrons. Remarkably, even at the highest field where a free electron would gain half the energy of the band-gap across a single lattice spacing, the forbidden gap largely exists. Existing lasers can easily exceed this limit, so it is important to develop a theoretical understanding of electronic structure in the nonperturbative limit.

SG and DAR are supported through the PULSE Institute at the SLAC National Accelerator Laboratory by the U.S. Department of Energy, Office of Basic Energy Science. DAR thanks Phil Bucksbaum for many fruitful discussions. The work at Ohio State University is funded by DOE contracts DE-FG02-06ER15833 and DE-FG02-04ER15614. LFD also acknowledges support from the Hagenlocker chair.

---

\* `shambhu@slac.stanford.edu`

† `dreis@slac.stanford.edu`

- [1] S. Ghimire, A. D. DiChiara, E. Sistrunk, P. Agostini, L. F. DiMauro, and D. A. Reis, *Nat Phys* **7**, 138 (2011).
- [2] L. Keldysh, *J. Exp. Theor. Phys.* **20**, 1307 (1965).
- [3] L. Keldysh, *J. Exp. Theor. Phys.* **20**, 1307 (1965).
- [4] K. B. Nordstrom, K. Johnsen, S. J. Allen, A.-P. Jauho, B. Birnir, J. Kono, T. Noda, H. Akiyama, and H. Sakaki, *Phys. Rev. Lett.* **81**, 457 (1998).
- [5] A. H. Chin, J. M. Bakker, and J. Kono, *Phys. Rev. Lett.* **85**, 3293 (2000).
- [6] A. H. Chin, O. G. Calderón, and J. Kono, *Phys. Rev. Lett.* **86**, 3292 (2001).
- [7] A. Srivastava, R. Srivastava, J. Wang, and J. Kono, *Phys. Rev. Lett.* **93**, 157401 (2004).
- [8] Y. Yacoby, *Phys. Rev.* **169**, 610 (1968).
- [9] A. P. Jauho and K. Johnsen, *Phys. Rev. Lett.* **76**, 4576 (1996).
- [10] V. E. Gruzdev, *J. Opt. Technol.* **73**, 385 (2006).
- [11] F. H. M. Faisal and J. Z. Kamiński, *Phys. Rev. A* **56**, 748 (1997).
- [12] N. Tzoar and J. I. Gersten, *Phys. Rev. B* **12**, 1132 (1975).
- [13] M. V. Ammosov, N. B. Delone, and V. P. Krainov, *J. Exp. Theor. Phys.* **64** (1986).
- [14] A. V. Mitrofanov, A. J. Verhoef, E. E. Serebryannikov, J. Lumeau, L. Glebov, A. M. Zheltikov, and A. Baltuska, *Phys. Rev. Lett.* **106**, 147401 (2011).
- [15] S. L. Chin, F. Yergeau, and P. Lavigne, *J. Phys. B: At. Mol. Phys* **18**, L213 (1985).
- [16] K. D. Schultz et al., *J. Mod. Opt.* **54**, 1075 (2007).
- [17] H. Yoshikawa and S. Adachi, *Jap. Journal of Appl. Phys.* **36**, 6237 (1997).
- [18] C. Klingshirn et al., *Phys. Status Solidi B* **247**, 1424 (2010).
- [19] P. H. Bucksbaum, R. R. Freeman, M. Bashkansky, and T. J. McIlrath, *J. Opt. Soc. Am. B* **4**, 760 (1987).
- [20] M. Goano, F. Bertazzi, M. Penna, and E. Bellotti, *J. of Appl. Phys.* **102**, 083709 (2007).
- [21] L. Keldysh, *J. Exp. Theor. Phys.* **34**, 788 (1958).

- [22] W. Franz, Z. Naturforsch **13**, 484 (1958).
- [23] Y. Mizumoto, Y. Kayanuma, A. Srivastava, J. Kono, and A. H. Chin, Phys. Rev. B **74**, 045216 (2006).
- [24] J. K. Wahlstrand and J. E. Sipe, Phys. Rev. B **82**, 075206 (2010).

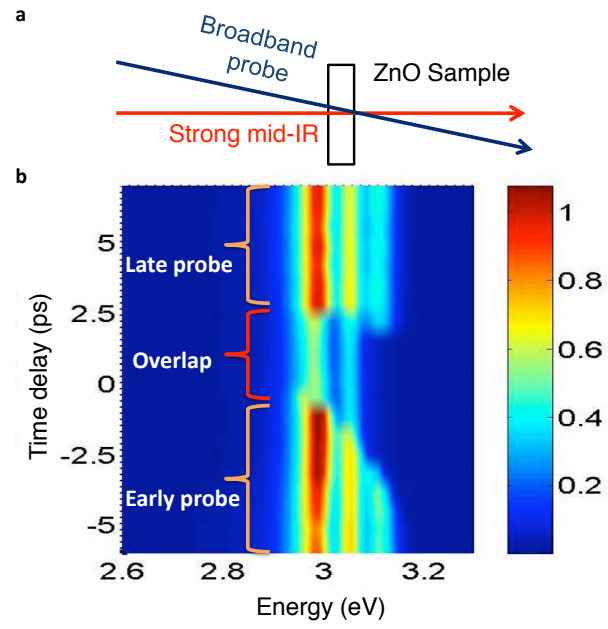


FIG. 1: (color online) Measurement of the field induced electroabsorption in a single crystal ZnO in the pump-probe geometry. (a) schematic of the pump-probe setup—a strong MIR beam centered at  $3.25 \mu\text{m}$  is focused on to the  $500 \mu\text{m}$  thick crystal near normal incidence and a weak broadband near band-gap optical probe intersect the pump at  $\sim 18$  degrees. (b) The measured transmitted probe light as a function of the pump-probe time delay at a MIR intensity of  $1 \text{ TW}/\text{cm}^2$ .

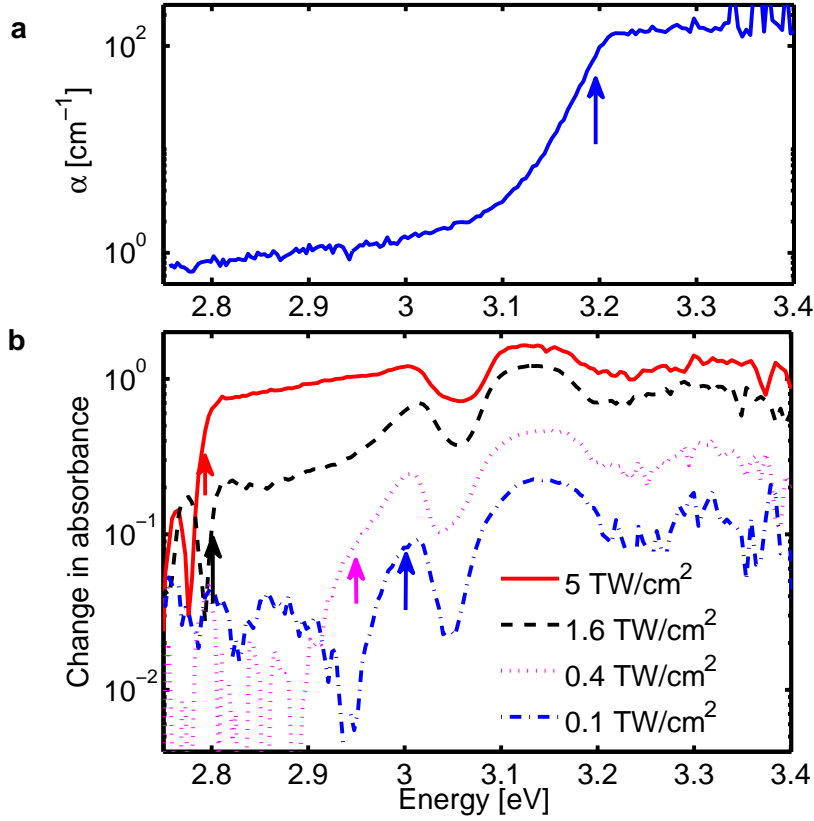


FIG. 2: (color online) MIR intensity dependence of the absorption in ZnO. (a) Measured field-free absorption coefficient of ZnO. Above  $\sim 3.2$  eV the measurement is limited by the dynamic range of the spectrophotometer for a  $500\mu\text{m}$  thick crystal. (b) relative increase in integrated absorbance in the presence of MIR laser, at intensities of 0.1, 0.4, 1.6, and 5.0  $\text{TW}/\text{cm}^2$  for a  $500\mu\text{m}$  crystal. Approximate location of absorption edges are marked by the vertical arrows.

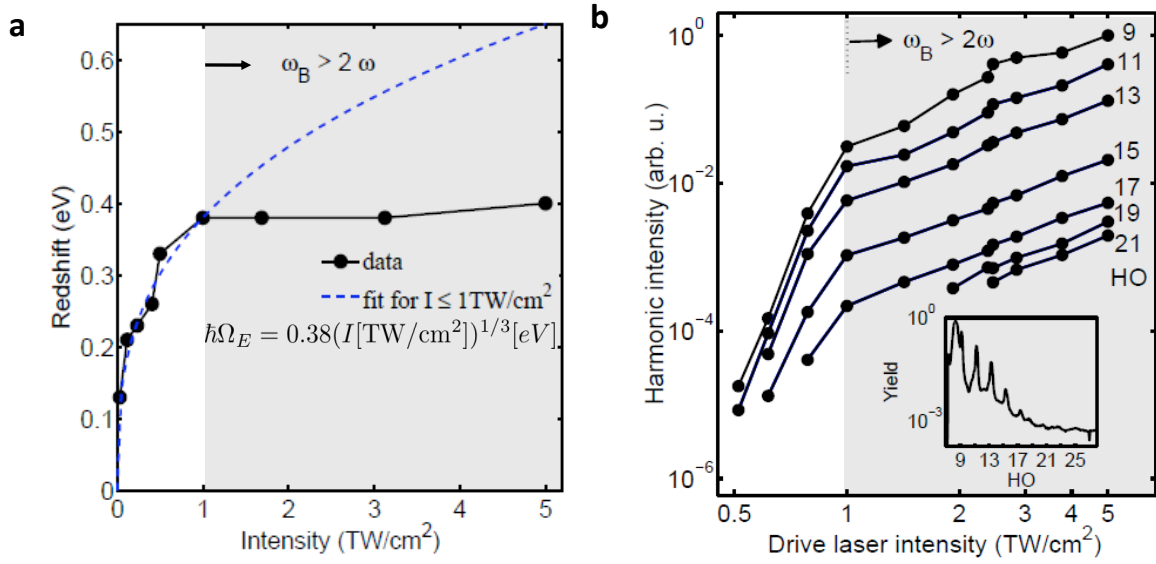


FIG. 3: (color online) (a) Scaling of the field induced redshift in the absorption edge for ZnO. The data fits a simple (Franz-Keldysh) model for photon assisted tunneling up to 1 TW/cm<sup>2</sup>. (b) Dependence of the yield of the MIR harmonics (HO 9-21) to the laser intensity. The individual harmonic yields show two distinct scalings to the drive laser intensity. A portion of the harmonic spectra collected from a 500  $\mu\text{m}$  thick ZnO crystal at 5 TW/cm<sup>2</sup> is shown in the inset. In both (a) and (b) the shaded region represents a high-intensity regime where the Bloch frequency exceeds twice the MIR frequency.